Karlsruher Institut für Technologie

Inert strength measurement on hot water soaked silica

Open Access am KIT

by Susanne Wagner[1], Beate Hohn[1], Dominic Creek[1], Michael J. Hoffmann[1], Gabriele Rizzi[1], Sheldon M. Wiederhorn[2], Theo Fett[1]

KIT SCIENTIFIC WORKING PAPERS 19

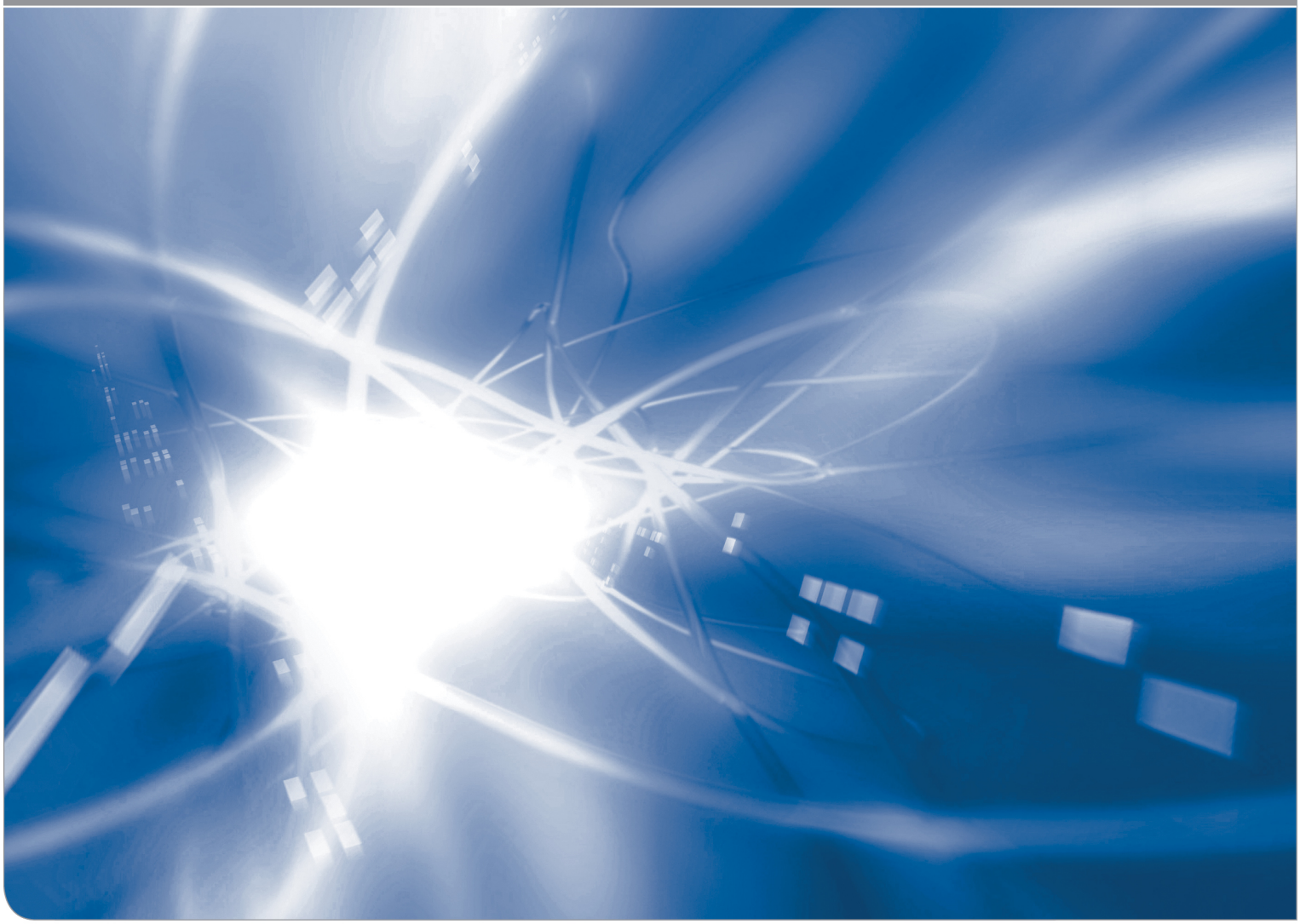

KIT – Universität des Landes Baden-Württemberg und nationales Forschungszentrum in der Helmholtz-Gemeinschaft

[1]Institut für Angewandte Materialien, Karlsruher Institut für Technologie (KIT)

[2]National Institute of Standards and Technology, Gaithersburg, MD

Impressum

Karlsruher Institut für Technologie (KIT)
www.kit.edu

2014

ISSN: 2194-1629

Abstract

The effect of water soaking on the strength of silica glass is studied. When silica glass is immersed in warm water and held there for an extended period of time, the strength increases over that of freshly damaged glass. The increase in strength is interpreted as the consequence of water diffusion into exposed surfaces of the test specimen, which results in swelling of the glass and shielding of cracks present in the surface of the glass. Experimental results are compared with theoretical predictions.

Contents

1. Introduction

In earlier publications [1, 2, 3, 4], we explored the idea that water can toughen silica glass by diffusing into the glass structure from the crack tip. This process sets up a negative stress intensity factor that shields the crack tip and enhances the strength of the specimen. Because diffusion rates increase with temperature, crack tip shielding should also increase as the temperature is increased, as should the specimen strength. Using the model presented in [2], we explored the mechanism of crack tip shielding and showed that the calculated changes in strength resulting from water exposure at 88 °C agreed sufficiently with experimental values measured on high-silicate glass Vycor by Ito and Tomozawa [5], and Hirao and Tomozawa [6]. The effects on inert strength at this rather low soaking temperature are only about 10%. In this paper, we will address the same phenomenon, but at higher temperatures, 250 ºC.

Strength measurements at 250°C are in principle known from literature. Li and Tomozawa [7] soaked silica bars for up to 4 days soaking time and tested the strengths in dynamic bending tests under subcritical crack growth conditions. To the authors' knowledge, So far no really inert strength measurements are available for silica.

1.1 Water diffusion in silica

Water diffusion into the surface of silica glass has been studied experimentally by a number of investigators, and shown to depend on temperature according to

$$D_w = A_0 \exp[-Q_w / R(T + 273°)] \tag{1}$$

where Q_w is the activation energy, (T+273°) is the absolute temperature, and R is the gas constant [8]. As reported in reference [8] for silica, Q_w = 72.3 kJ/mol, $\log_{10} A_0$ = -8.12 (A_0 is in m^2/s) for the *effective* diffusivity in the temperature range 0 °C to 200 °C).

The diffusion distance b, an appropriate measure for the thickness of the diffusion zone (where the water concentration is roughly half of that at the surface) is given by

$$b = \sqrt{D_w t} \tag{2}$$

with the time t after the first water contact.

The water in the diffusion zone reacts with the silica network according to

$$\equiv\text{Si-O-Si}\equiv + H_2O \leftrightarrow \equiv\text{SiOH+HOSi}\equiv \tag{3}$$

with the mobile molecular water H_2O and the immobile hydroxyl groups SiOH. If the concentration of the hydroxyl is denoted as S = [≡SiOH] and that of the molecular water C = [H_2O], these sum of the two species of "water" result in the total water solubility C_w

$$C_w = C + \tfrac{1}{2} S \tag{4}$$

Water diffusion into the surface of silica glass in the temperature range of 23°C ≤ $T \leq 200$°C was studied experimentally by Zouine *et al.* [8]. From this paper and the derivation in [4], the hydrogen concentration at the surface can be calculated as

$$C_w \cong \tfrac{1}{2} 1.15 \times 10^{20}\, cm^{-3} \exp[0.009T] \qquad (5)$$

This dependency is plotted in Fig. 1a. Here the solid curve represents the strengths for the region in which D and c_0 were measured, the dashed curve parts show the temperature range in which these parameters were extrapolated. The squares represent the measurements by Zouine et al. [8]. Also for higher soaking temperatures up to 250°C, Eq.(5) may be used as an approximation.

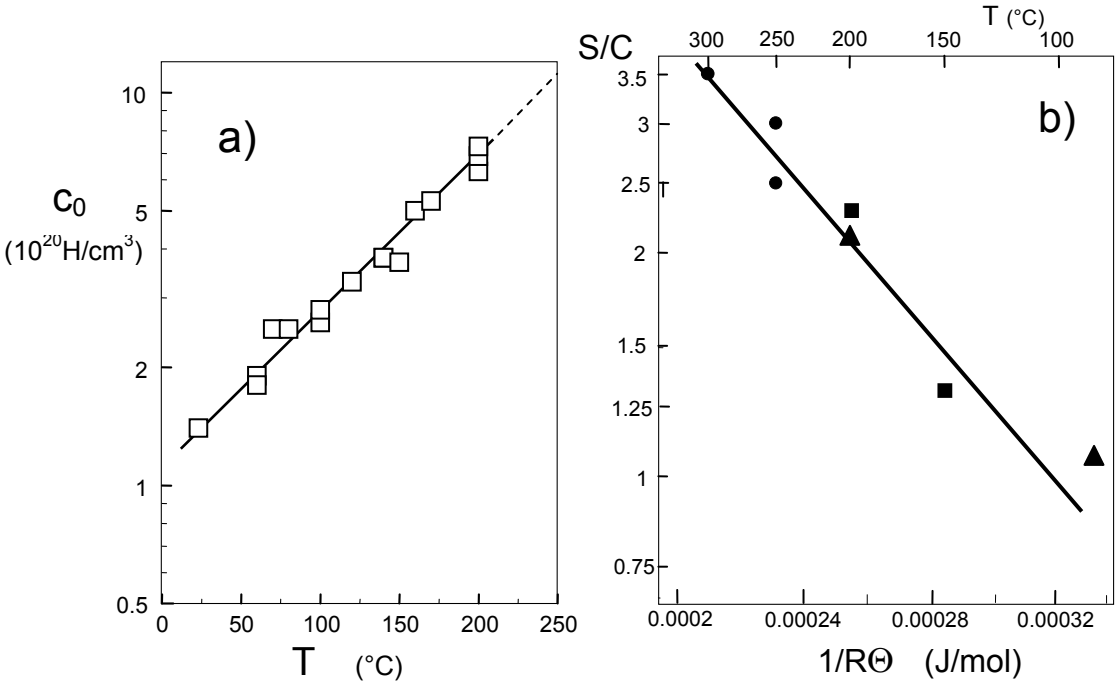

Fig. 1 Temperature dependence of hydrogen concentration at the surface from Zouine et al. [8], b) the occurrence of hydroxyl and molecular water species in the glass ahead of a crack tip, squares: from Zouine et al.[8], circles: from Tomozawa and co-workers [12-14], triangles: from Wiederhorn et al. [15].

1.2 Volume swelling

From measurements by Shelby [9], Shackelford [10], and Brückner [11] at temperatures >1000°C it could be concluded that water entrance results in a volume expansion. Since the water at such high temperatures is practically present by 100% in the form of silicon hydroxide, [SiOH]≡*S*, the experimental results on swelling by water at least hold for the hydroxide species. So far no information on volume increase is available for the molecular water [H_2O]≡*C*. Therefore, the authors tentatively used the same swelling for both of the water species [1-4].

In the following considerations let us now consider the case of different swelling behavior for the hydroxyl and the molecular water. The total swelling strain ε_v is then

composed by the individual contributions of the hydroxyl and the molecular water according to the rule of mixture

$$\varepsilon_v = \frac{S/2}{C+S/2}\varepsilon_S + \frac{C}{C+S/2}\varepsilon_C, \tag{6}$$

where ε_v is the total volume strain due to Eq. 3, ε_S is the volume strain due to the presence of *S/2* moles of ≡SiOH in a volume of the glass containing *C*+*S/2* moles of glass, ε_C is a similar definition for interstitial molecular water.

The ratio *S*/*C* as a function of temperature can be seen from measurements by (Zouine et al. [8] (squares in Fig. 1b), Tomozawa et al. [12, 13, 14], (circles), and Wiederhorn et al. [15], (triangles). A fit relation for the experimental results is

$$k = \frac{S}{C} = A\exp\left(\frac{-Q_1}{R\Theta}\right) \tag{7}$$

with the absolute temperature Θ=273°+*T*, *A*=32.3 and *Q*=10.75 kJ/mol. For *T*=250°C it results *S*/*C*=2.78 (open square in Fig. 1b).

In the past, there was no information on the swelling strains for molecular water available. Therefore, we assumed in [1-4] that *S* and *C* might cause the same effect. From recent measurements of deformation by swelling stresses [15] it is suggested that $\varepsilon_S >> \varepsilon_C$.
Therefore, we assume that the actually unknown contribution by molecular water, ε_C, may disappear completely resulting in

$$\varepsilon_C = 0 \Rightarrow \varepsilon_v = \frac{S/2}{C+S/2}\varepsilon_S \tag{8}$$

Due to the proportionality of water concentration and swelling strain, the volume strain for silicon hydroxyl can be written as

$$\varepsilon_v \cong 0.00147\frac{S/2}{C+S/2}\exp[0.009T] \tag{9}$$

as derived in [4].

A volume element near the surface that undergoes swelling cannot freely expand. If the diffusion zone is small compared to the component dimensions, expansion is completely prevented in the surface plain and can only take place normal to the surface. This results in the compressive equi-biaxial swelling stress at the surface [16]

$$\sigma_0 = -\frac{\varepsilon_v E}{3(1-\nu)} \tag{10}$$

where *E* is Young's modulus and ν Poisson's ratio.

2 Computation of the total stress intensity factor for a surface crack

As in the earlier publication [4] we begin our analysis by estimating the magnitude of the total stress intensity factor, K_{tot}, experienced by the critical crack during the strength test. The total stress intensity factor consists of three contributions: K_{app}, which is primarily the result of the applied stresses and the geometry of the crack; K_{sh} which results from water penetration into the fresh fracture surfaces and the other surfaces of the fracture specimen. The condition for crack growth is $K_{tot} \geq K_{Ic}$.

In order to provide a transparent analysis we restricted the possible aspect ratios, to the commonly chosen semi-circular surface crack with the depth given by a (Fig. 2) and an aspect ratio of a/c=1. The plane of the crack is assumed to be perpendicular to the specimen length axis.

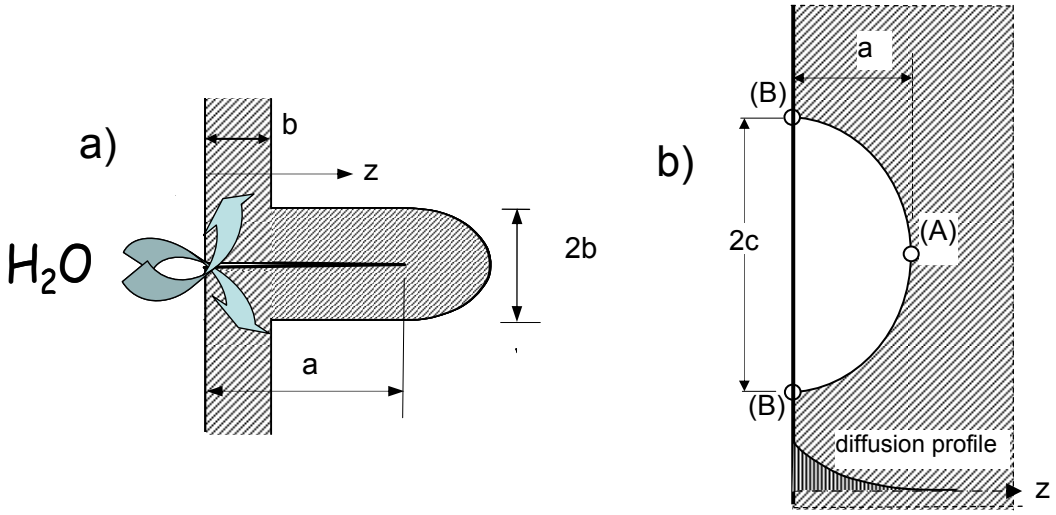

Fig. 2 Single failure relevant crack in an infinite body exhibiting a diffusion and swelling zone, a) side view, b) top view on the semi-elliptical surface crack.

The applied stress intensity factor given by Eq. 11 and Eq. 12 below were derived and discussed in [17] for the case of straight specimen surfaces. Since the initial natural surface cracks are very small compared to the specimen thickness W, a/W<<1,it holds for the stress intensity factor at the deepest point (A)

$$K_{appl,A} = \sigma_{appl} 1.173 \sqrt{a} \tag{11}$$

and for the surface points (B)

$$K_{appl,B} = \sigma_{appl} 1.29 \sqrt{a} \ , \tag{12}$$

where in bending tests σ_{appl} is the outer fiber tensile stress. This solution can also be used for cylindrical specimens if the crack depth is small compared with the cylinder radius, a/R<<1. As outlined in reference [4] for the current experiment, $a/R \leq 0.01$; the crack is assumed to be at the midpoint of the test specimen, with one axis perpen-

dicular to the specimen length axis and the other principal axis in the plane of the specimen surface.

As noted above, two contributions make up the shielding stress intensity factor: one coming from the diffusion zone originating from the crack faces, the second originating from the external surfaces of the specimen.

The shielding stress intensity factors at the deepest point A and the surface points B, $K_{sh,\,A}$ and $K_{sh,\,B}$, are for $b<<R$ [4] and $0.15<b/a<1.25$

$$K_{sh,A} \cong 1.17\sqrt{a}\,\sigma_0 \tanh\left(0.698\sqrt{\frac{b}{a}} + 0.317\frac{b}{a}\right) \tag{13}$$

and

$$K_{sh,B} \cong 1.29\sqrt{a}\,\sigma_0 \tanh\left(1.327\sqrt{\frac{b}{a}} + 0.064\frac{b}{a}\right) \tag{14}$$

3. Toughness and inert strength

3.1 Apparent Toughness

The total stress intensity factors including shielding are given by

$$K_{tot,A} = K_{sh,A} + K_{appl,A} \tag{15a}$$

$$K_{tot,B} = K_{sh,B} + K_{appl,B} \tag{15b}$$

where $K_{appl,A}$ and $K_{appl,B}$ are obtained from eq.(11) and eq.(12); $K_{sh,A}$ and $K_{sh,B}$, from eq.(13) and eq.(14). The applied stress intensity factors for inert tests have to be computed using the initial crack dimensions a_0 and c_0.

The shielding effect is responsible for an apparent increase of the fracture toughness which is, in general, identified with the applied stress intensity factor at failure, $K_{\mathrm{appl,cr}}$. From eqs.(15) the *apparent fracture toughness*, in the following denoted as $\hat{K}_{\mathrm{Ic}}$, simply results as

$$\hat{K}_{\mathrm{Ic}} = K_{appl,cr} = K_{\mathrm{Ic}} - K_{sh} \tag{16}$$

Since $K_{\mathrm{sh}}<0$, it holds $\hat{K}_{\mathrm{Ic}}>K_{\mathrm{Ic}}$. On the other hand it becomes clear from the fact that the inert strengths are proportional to the applied stress intensity factor, $\sigma_{\mathrm{c}} \propto K_{\mathrm{appl,cr}}$, that the two properties increase by the same factor. In the following considerations, we therefore concentrate on the strength, exclusively. The apparent toughness for the surface points and the deepest point of a semi-circular crack is shown in Fig. 3a.

3.2 Inert strength

Using the temperature dependent swelling strain together with the temperature effect on the diffusivity, the inert strengths could be computed as a function of T in the same way as outlined in [4]. The inert strength, σ_c, is given by the condition

$$\sigma_c = \mathrm{Min}\left(\frac{K_{\mathrm{Ic}} - K_{sh,A}}{1.17\sqrt{a}}, \frac{K_{\mathrm{Ic}} - K_{sh,B}}{1.29\sqrt{a}} \right) \tag{17}$$

Strength predictions are shown in Fig. 3b. For this purpose initial inert strengths were assumed to be σ_c=100, 150, and 200 MPa. From Fig. 3b an effect of water swelling is predicted which gives a strength increase by a factor of about 2 for 250°C depending on the soaking time.

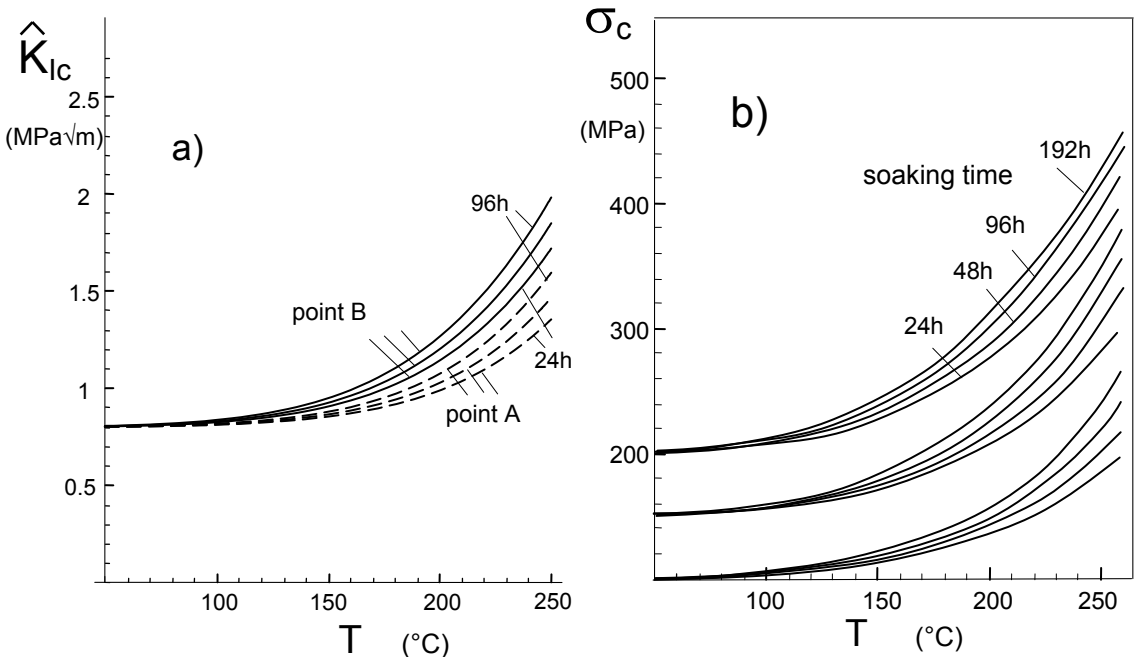

Fig. 3 a) Apparent fracture toughness $\hat{K}_{Ic}$ after hot-water soaking for a semi-circular crack of 30 µm depth, b) calculated inert strengths as a function of water-soaking temperature T and soaking time, predicted for inert strengths of σ_c=100, 150, and 200 MPa for freshly abraded test specimens.

4. Strength measurements

We studied strength behaviour on the silica glass EN08NB (GVB, Herzogenrath) containing 99.98% SiO_2. Cylindrical bending bars of 45 mm length were cut from silica rods of 4 mm diameter, maintaining the original gleam surface from manufacturing.

Then all specimens were annealed for 1h at 1150°C in vacuum to eliminate residual surface stresses introduced by cooling from melting temperature. In order to avoid any water contact, the series intended for strength measurements in an inert environment were stored in fresh silicon oil immediately after cooling as proposed by Sglavo and Green [18] who considered the silicon oil to be an inert medium.

Bending strength tests were carried out in liquid nitrogen in a 3-point testing device to avoid any interaction of the specimen with water in the environment. The results for specimens soaked soaked for 192h at 260°C, compared to unsoaked specimens (circles)

are shown in Fig. 4 in a Weibull representation. The distribution of the unsoaked specimens shows the expected Weibull straight-line with a Weibull modulus of m = 12.3 and a characteristic strength $\sigma_0 = 171.3$ MPa both obtained by application of the Maximum Likelihood procedure [19].

From the median strength of $\sigma_{med} \cong 160.6$ MPa and the fracture toughness of K_{Ic}=0.8 MPa√m [20], a median initial crack depth of a_0 = 14.9 µm can be concluded. This value is less than the water penetration depth of $b \cong 21$µm under soaking conditions; thus, the cracks are fully embedded in the diffusion/swelling zone.

The soaked specimens show clearly larger strengths. In contrast to the unsoaked specimens, the soaked specimens exhibit a bimodal distribution caused by two different flaw populations. The Weibull distributions of the flaw populations "1" and "2" are given by

$$F_1 = 1 - \exp\left[-\left(\frac{\sigma_c}{\sigma_{01}}\right)^{m_1}\right] \tag{18}$$

and

$$F_2 = 1 - \exp\left[-\left(\frac{\sigma_c}{\sigma_{02}}\right)^{m_2}\right] \tag{19}$$

with the two different characteristic strengths σ_{01} and σ_{02} and the related Weibull exponents m_1 and m_2. Superposition of these flaws results in the total failure probability (for details see e.g. [21], Section 8)

$$F = F_1 + F_2 - F_1 F_2 = 1 - \exp\left[-\left(\frac{\sigma_c}{\sigma_{01}}\right)^{m_1} - \left(\frac{\sigma_c}{\sigma_{02}}\right)^{m_2}\right] \tag{20}$$

The Weibull parameters obtained by curve-fitting according to eq. (20) are compiled in Table 1.

Flaw population "1"		Flaw population "2"		
m_1	σ_{01} (MPa)	m_2	σ_{02} (MPa)	Confidence Level
21.4	437.5 [435, 439]	2.7	394 [388, 400]	10%
21.4	437.5 [425, 450]	2.7	394 [362, 427]	50%
21.4	437.5 [404, 471]	2.7	394 [306, 482]	90%

Table 1: Weibull parameters for the water soaked specimens with confidence intervals for characteristic strengths.

The curve fit according to eq. (20) is introduced in Fig. 4 by the solid curve. The dash-dotted straight lines give the asymptotes representing the individual flaw populations.

Due to their high strengths, the soaked specimens shattered in more than two fracture pieces (mostly 4-6 fragments). Therefore, it was not possible to carry out a fractographic study on the broken test pieces.

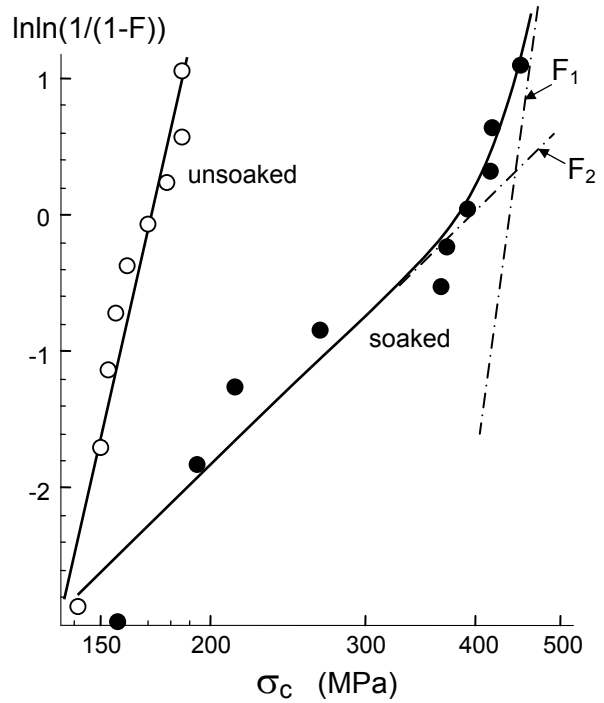

Fig. 4 Inert strengths measured on cylindrical bending bars in liquid N_2 under 3-point bending load (triangles: median values)

5. Strength predictions

Measurements in liquid nitrogen showed a strong increase of the inert strength. The results of Fig. 4 are plotted once more in Fig. 5 together with the predictions according to eqs.(11-17). The predictions for the 10 soaked specimens were based on the Weibull distribution for the unsoaked specimens. First, the strength of the n^{th} specimen was computed for a total number of N specimens via

$$\sigma_n = \sigma_0 \left(\ln \frac{1}{1-(n-0.5)/N} \right) \tag{21}$$

For each selected specimen, the eqs.(11-17) were applied resulting in the predicted strength of soaked specimen corresponding to the same failure probability F. This procedure yields the solid red curve in Fig. 5. This curve is slightly curved, but can, nevertheless, be approximated by a Weibull straight line. Application of the Maximum Likelihood procedure results in the dashed line represented by the characteristic strength of $\sigma_0 = 414$ MPa and the Weibull modulus $m = 20.3$.

predicted		measured		
m_1	σ_{01} (MPa)	m_1	σ_{01} (MPa)	Confidence Level
20.3	413.8	21.4	437.5 [425, 450]	50%
20.3	413.8	21.4	437.5 [404, 471]	90%

Table 2: Comparison of Weibull parameters for the predicted characteristic strengths of flaw population "1" with measurements.

Good agreement can be stated between the prediction and the measurements for the soaked specimens as can be seen from the comparison made in Table 2. The predicted strength is about 95% of the measured one.

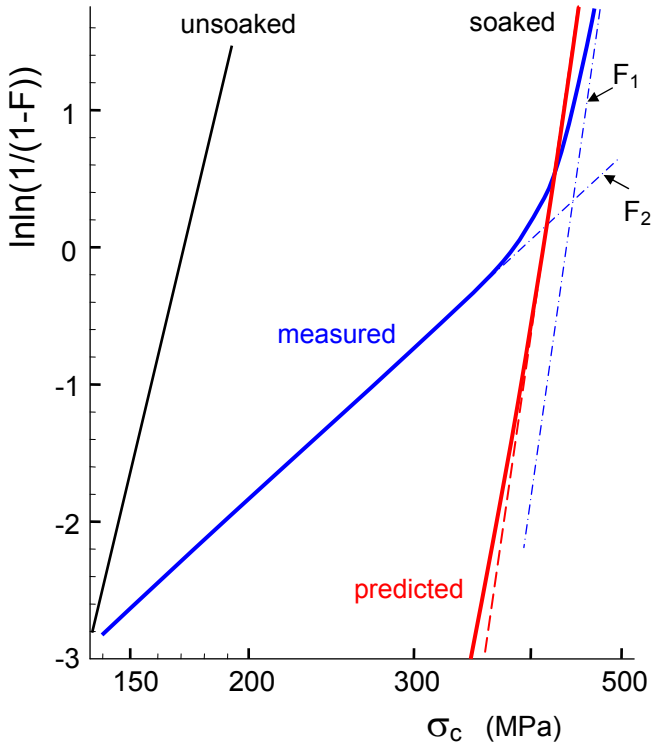

Fig. 5 Strengths of water-soaked specimens (red curve) predicted from the strengths of the unsoaked specimens (black Weibull line) by application of eqs.(11)-(17), red dashed straight-line: predicted strengths fitted by a Weibull distribution, blue curve: measured strength of soaked specimens from Fig. 4 together with asymptotes given by the blue dash-dotted lines.

6. Discussion

From the nearly linear shape of the strength distribution of unsoaked specimens in the Weibull plot, we conclude that the initial cracks responsible for failure were also Weibull distributed.

The bimodal strength distribution of the soaked specimens calls for an interpretation by a superposition of surface and volume flaws as observed e.g. by Bansal et al. [22, 23] (see also [21]).

In order to discuss the observed curve shape, let us assume the coexistence of the surface defects (cracks) and inner flaws (pores) as schematically illustrated in Fig. 6a. The blue line indicates the strengths for the surface cracks, whereas the red line gives the strengths for the pores.

Under normal circumstances, the specimens will fail at the surface, because the strength is lowest there. Failure starting from internal defects is rare, and can occur only when the two curves intersect at a very small failure probability F.

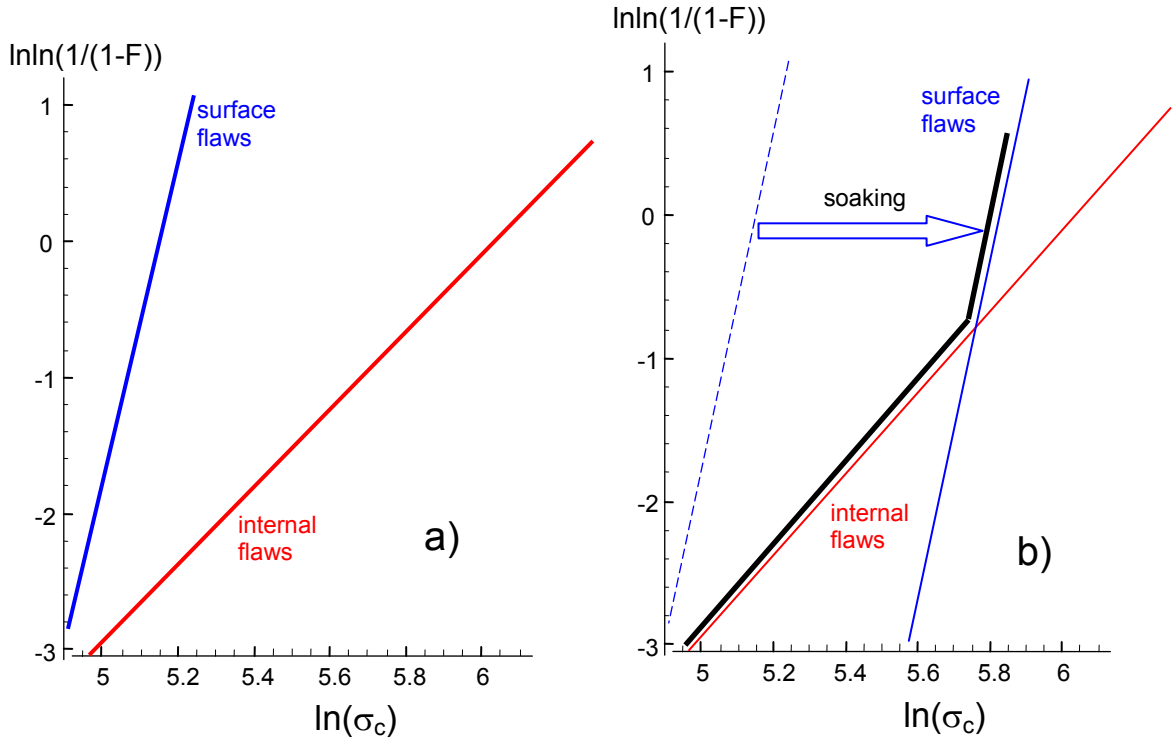

Fig. 6 a) Strength for failure starting at the surface flaws and at inner defects, b) shift of the surface strength by soaking resulting in a bimodal strength curve.

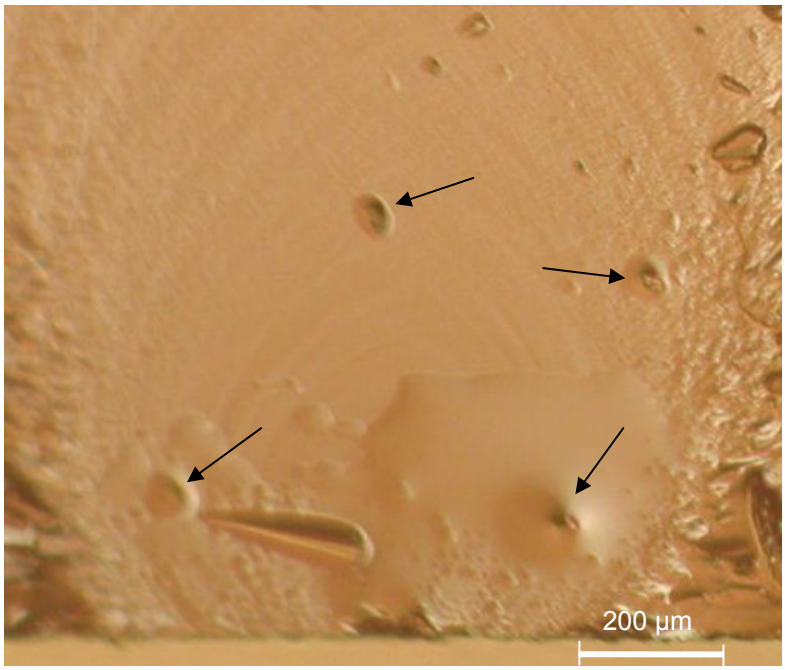

Fig. 7 Fracture surface for a test in lab air at room temperature showing pore-like internal defects, some of them indicated by arrows.

Soaking the specimen strengthened its surface and the blue dotted line in Fig. 6b shifted to higher strength values as indicated by the arrow. The measurable strength is the minimum of the shifted blue and the red line. This results in the kinked black curve observed in our measurements. Figure 7 shows some internal pore-like defects

obtained from strength measurements at room temperature where only two fragments occurred that allowed microscopic inspection.

Figure 8 shows the predicted strength in comparison with the measured strength. Since the strength increase (strength with soaking minus strength of unsoaked specimens) should be proportional to the swelling strains according to eqs. (10), (13), (14), and (17), its value represents reflects the amount of swelling.

The ratio of the predicted to measured strength

$$\frac{(\sigma_{c,soaked} - \sigma_{c,unsoaked})_{predicted}}{(\sigma_{c,soaked} - \sigma_{c,unsoaked})_{measured}} = \frac{(\sigma_{sw})_{predicted}}{(\sigma_{sw})_{measured}} = \frac{(\varepsilon_{sw})_{predicted}}{(\varepsilon_{sw})_{measured}} \tag{22}$$

is plotted in Fig. 8 as the square together with the ratio of the predicted and measured bending moments by water soaking according to [15]. The square represents the ratio for the characteristic strength values σ_0 from Tables 1 and 2, namely, (413.8-171.3) / (437.5-171.3) = 0.91. The 90%-confidence interval of Table 1 yields the perpendicular bar.

The filled in circles in Fig. 8 show the agreement between direct measured bending moments due to swelling with theoretical predictions according to eqs. (8-10) reported in [15]. It has to be noted that the indirect evaluation via inert strength measurements confirms conclusions from the direct measurement of bending moments and swelling stresses.

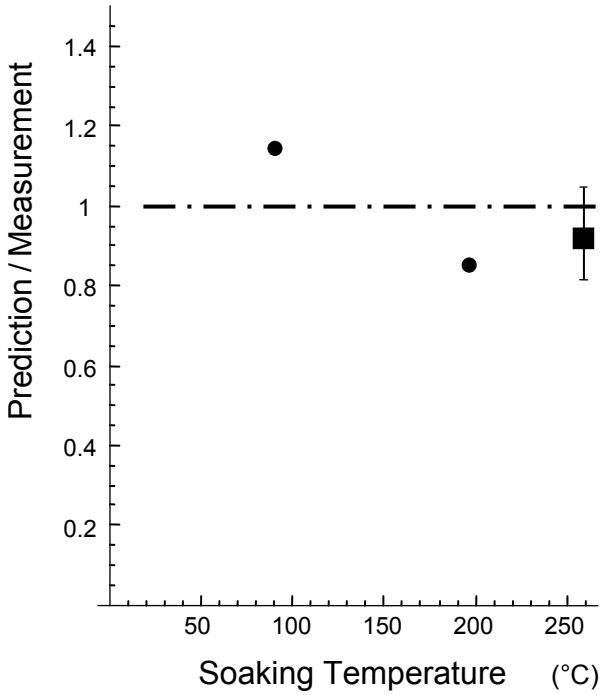

Fig. 8 Predicted and measured swelling effects: Circles – a comparison of the measured bending moment with calculations based on measured concentrations water in silica glass and the volume expansion results in [15], square: ratio of the swelling contributions according to eq. (22) with the bar representing the 90%-convidence interval in Table 1.

References

1. S.M. Wiederhorn, T. Fett, G. Rizzi, S. Fünfschilling, M.J. Hoffmann and J.-P. Guin, "Effect of Water Penetration on the Strength and Toughness of Silica Glass," *J. Am. Ceram. Soc.* **94** (2011) [S1], 196-203.
2. S.M. Wiederhorn, T. Fett, G. Rizzi, M.J. Hoffmann and J.-P. Guin, "The Effect of Water Penetration on Crack Growth in Silica Glass," *Engng. Fract. Mech.* **100** (2013), 3-16.
3. S.M. Wiederhorn, T. Fett, G. Rizzi, M. Hoffmann, J.-P. Guin, "Water Penetration – its Effect on the Strength and Toughness of Silica Glass," *Met. Mater. Trans. A*, **44**(2013) [3], 1164 -1174.
4. T. Fett, G. Rizzi, M. Hoffmann, S. Wagner, and S.M. Wiederhorn, "Effect of Water on the inert Strength of Silica Glass: Role of Water Penetration," *J. Am. Ceram. Soc.* **95**(2012) [12], 3847-3853.
5. S. Ito and M. Tomozawa, "Crack Blunting of High-Silica Glass," *J. Am. Ceram. Soc.* **65**(1982) [8], 368-371.
6. K. Hirao and M. Tomozawa, "Dynamic Fatigue of Treated High-Silica Glass: Explanation by Crack Tip Blunting," *J. Am. Ceram. Soc.* **70**(1987) [6], 377-82.
7. H. Li and M. Tomozawa, "Mechanical strength increase of abraded silica glass by high pressure water vapor treatment," *J. Non-Cryst. Solids* **168**(1994), 287-292.
8. Zouine, A., Dersch, O., Walter, G., Rauch, F., "Diffusivity and solubility of water in silica glass in the temperature range 23-200°C," *Phys. Chem. Glasses*, **48** (2007), 85-91.
9. Shelby, J.E., "Density of vitreous silica," *J. Non-Cryst*. **349**(2004)**,** 331-336.
10 Shackelford, J.F., Masaryk, J.S., Fulrath, R.M., *J. Am. Ceram. Soc*. **53**(1970), 417.
11 Brückner, R., *J. Non-Cryst.* **5**(1971), 281.
12 Wakabayashi, H., Tomozawa, M., "Diffusion of water into silica glass at low temperature," J. Am. Ceram. Soc. **72**(1989), 1850-55.
13 Davis, K., Tomozawa, M., "An infrared spectroscopic study of water-related species in silica glasses," *J. Non-Cryst. Solids*, **201**(1996), 177-198.
14 Oehler, A., Tomozawa, M., "Water diffusion into silica glass at low temperature under high water pressure" *J. Non-Cryst. Solids*, **347**(2004), 211-219.
15 S. M. Wiederhorn, F. Yi, D. LaVan, T. Fett, M.J. Hoffmann, "Volume Expansion caused by Water Penetration into Silica Glass," *J. Am. Ceram. Soc*. In review.
16 S.P. Timoshenko and J.N. Goodier, *Theory of Elasticity,* Third Edition, McGraw-Hill, Inc, New York (1987), Chapter 13.
17. J.C. Newman and I.S. Raju, "An empirical stress intensity factor equation for the surface crack," *Engng. Fract. Mech.* **15,** 185-192, (1981).
18 V.M. Sglavo and D.J. Green, "Fatigue limit in fused silica," *J. Eur. Cram. Soc.* **21** (2001) 561-567.
19 Lawless, J.F. (1982) *Statistical Models and Methods for Lifetime Data*, Wiley, New York.
20 S.M. Wiederhorn, "Fracture Surface Energy of Glass," *J. Am. Ceram. Soc*., **52**[2], 99-105, (1969).
21 Munz, D., Fett, T. (1999), *CERAMICS, Failure, Material Selection, Design,* Springer-Verlag, Heidelberg.
22 Bansal, G.K., Duckworth, W.H., Niesz, D.E., "Strength-size relations in ceramic materials: Investigation of an alumina ceramic," *J. Am. Ceram. Soc.* **59** (1976), 472–478.
23 Bansal, G.K., Duckworth, W.H., Niesz, D.E., *Strength analysis of brittle materials*, Battelle-Report, Columbus, (1976).

KIT Scientific Working Papers
ISSN 2194-1629

www.kit.edu